Letter

Spin squeezing with itinerant dipoles: A case for shallow lattices

David Wellnitz,[1,2,*] Mikhail Mamaev,[1,2] Thomas Bilitewski,[3] and Ana Maria Rey[1,2]
[1]*JILA, National Institute of Standards and Technology and Department of Physics, University of Colorado, Boulder, Colorado 80309, USA*
[2]*Center for Theory of Quantum Matter, University of Colorado, Boulder, Colorado 80309, USA*
[3]*Department of Physics, Oklahoma State University, Stillwater, Oklahoma 74078, USA*

(Received 4 January 2023; revised 11 October 2023; accepted 2 January 2024; published 7 February 2024)

Entangled spin squeezed states generated via dipolar interactions in lattice models provide unique opportunities for quantum enhanced sensing and are now within reach of current experiments. A critical question in this context is which parameter regimes offer the best prospects under realistic conditions. Light scattering in deep lattices can induce significant decoherence and strong Stark shifts, while shallow lattices face motional decoherence as a fundamental obstacle. Here we analyze the interplay between motion and spin squeezing in itinerant fermionic dipoles in one dimensional chains using exact matrix product state simulations. We demonstrate that shallow lattices can achieve more than 5 dB of squeezing, outperforming deep lattices by up to more than 3 dB, even in the presence of low filling, loss, and decoherence. We relate this finding to SU(2)-symmetric superexchange interactions, which keep spins aligned and protect collective correlations. We show that the optimal regime is achieved for small repulsive off-site interactions, with a trade-off between maximal squeezing and optimal squeezing time.

DOI: 10.1103/PhysRevResearch.6.L012025

Introduction. Dipolar quantum gases made from polar molecules, Rydberg atoms, or magnetic atoms are emerging as promising platforms for near-term quantum technologies [1–6]. These systems are now routinely cooled to ultralow temperatures [7–18], and recently pushed into a new regime where individual particles can be controlled and measured using, e.g., quantum gas microscopes or optical tweezers [19–24].

Taking advantage of these impressive developments defines a new frontier for quantum enhanced sensing. Of particular importance in this context is spin squeezing [25,26], which quantifies the reduction of uncertainty along a measurement axis due to quantum correlations [27] and also serves as a probe for many-body entanglement [27–29]. While spin squeezing used to be exclusively generated using collective interactions accessible via photon or phonon mediated interactions or effectively in Bose-Einstein condensates [30–44], a new frontier [45–48] is the generation of spin squeezing in systems with power-law decaying interactions [19,21–24,49–54]. In this new paradigm, while spin squeezing up to 4 dB has been recently reported in systems with frozen particles [55–58], the generation of spin squeezing in itinerant systems can open new important opportunities, since it could help overcome the low filling fraction constraints and additional dephasing introduced by the tight trapping conditions needed to suppress motion.

Itinerant systems of polar molecules, confined in stacks of 2D pancakes already realized experimentally [59], have been considered as a promising setting for entanglement generation [60]. However, at currently achievable temperatures, inelastic and lossy collisions in the pancakes [61–67] give rise to motional dephasing and particle loss [59]. The latter could be significantly mitigated by imposing additional lattices along the 2D pancakes resulting in effective 1D arrays, which we investigate in this work.

Specifically, we study the exact quantum dynamics of fermionic itinerant dipoles trapped in a 1D chain using matrix product states (MPS). In all cases considered, which start with an initial spin coherent state, we find that spin squeezing and coherence times can be increased by reducing the lattice depth. For shallow lattices, particles remain itinerant [68,69], reducing positional disorder at nonunit filling fractions, $0 < f < 1$, while undesirable on-site lossy collisions can be suppressed by the quantum Zeno effect [49,70,71]. Figure 1(c) summarizes these main results. We further find that squeezing is enhanced when the signs of nearest neighbor dipole-dipole interactions and on-site interactions match, such that superexchange and dipole-dipole interactions add up. Smaller dipolar interactions give rise to larger squeezing, albeit at the cost of slower dynamics. We qualitatively explain these effects in a spin model valid for unit filling and sufficiently small tunneling. We also find that dephasing noise, e.g., due to differential lattice polarizability, can be echoed away, as observed in recent experiments [59], without affecting squeezing dynamics. Even though we focus the analysis on polar molecules, our predictions apply to generic itinerant fermionic systems featuring both contact and short-range off-site interactions.

*Corresponding author: david.wellnitz@colorado.edu

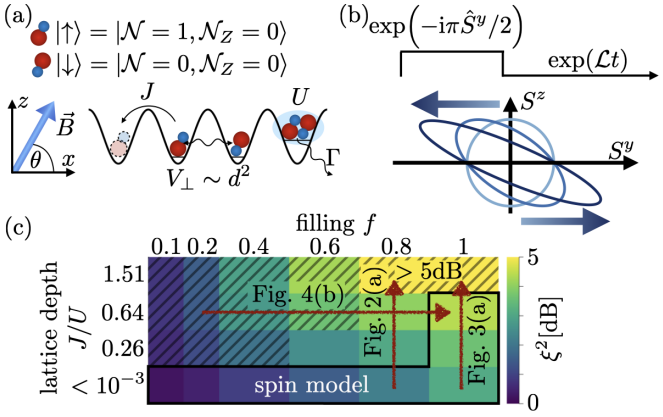

FIG. 1. (a) Schematic of the system (see text). (b) Top: Ramsey pulse sequence. Bottom: Schematic illustration of squeezing dynamics in the S^y-S^z plane. (c) Maximal squeezing ξ^2 for $t < 10$ ms versus filling fraction f and lattice depth. In x and y/z directions $(V_{\mathrm{latt},x}, V_{\mathrm{latt},\perp})/E_R = (3,3), (3,40), (5,40), (40,40)$ [$E_R = 2\pi^2\hbar^2/(m\lambda^2)$ is the recoil energy] (top to bottom, see the Supplemental Material for detailed parameters [72]). The black line indicates where the system can be approximated by a spin model. The striped area indicates where squeezing is growing past 10 ms.

Model. We consider an infinite 1D chain of fermionic dipoles trapped in an optical lattice with a spin-1/2 degree of freedom, which can, for example, be realized in the rotational states of molecules as $|\uparrow\rangle = |\mathcal{N}=1, \mathcal{N}_Z=0\rangle$ and $|\downarrow\rangle = |\mathcal{N}=0, \mathcal{N}_Z=0\rangle$, where a weak external field (electric field $\vec{E}$ or magnetic field $\vec{B}$) defines a preferred polarization axis [see Fig. 1(a)]. The system is modeled as an extended Fermi-Hubbard (FH) model with Hamiltonian $\hat{H} = \hat{H}_{\mathrm{FH}} + \hat{H}_{\mathrm{dip}}$ [73,74].

Here, $\hat{H}_{\mathrm{FH}}$ is the single-band FH Hamiltonian describing tunneling and on-site dipolar and contact interactions. It reads

$$\hat{H}_{\mathrm{FH}} = -\sum_{j,\sigma} J_\sigma (\hat{b}^\dagger_{j,\sigma}\hat{b}_{j+1,\sigma} + \mathrm{H.c.}) + U\sum_j \hat{n}_{j\uparrow}\hat{n}_{j\downarrow}, \quad (1)$$

with fermionic annihilation operators on site j with spin σ, $\hat{b}_{j,\sigma}$, and number operators $\hat{n}_{j\sigma} = \hat{b}^\dagger_{j,\sigma}\hat{b}_{j,\sigma}$. The tunneling rates J_σ and the contact interaction U_{contact} are controlled by the optical lattice depth, while the on-site dipolar interactions U_{dd} can be tuned via lattice depth, lattice anisotropy, and electric field ($U = U_{\mathrm{contact}} + U_{\mathrm{dd}}$). Even for shallow lattices considered here, the interaction-induced cross-band coupling is weak, justifying a single band approximation [72]. In general, a differential polarizability of the rotational states leads to spin-dependent tunneling rates, which can be tuned by the lattice polarization axis and are equal at a magic angle [75]. Close to zero field, the states $|\uparrow\rangle$ and $|\downarrow\rangle$ do not feature induced dipole moments and the interactions between dipoles on different lattice sites are characterized by a pure exchange Hamiltonian $\hat{H}_{\mathrm{dip}} = \sum_{i>j}\frac{1}{|j-i|^3}V_\perp(\hat{s}^x_i\hat{s}^x_j + \hat{s}^y_i\hat{s}^y_j)$. In 1D geometries for the parameters considered, the $1/r^3$ tail of the interactions speeds up the dynamics, but leaves the maximum attainable squeezing unchanged within numerical precision [72]. Because of that we approximate the Hamiltonian by the simpler nearest neighbor model:

$$\hat{H}_{\mathrm{dip}} = V_\perp \sum_j \left(\hat{s}^x_j\hat{s}^x_{j+1} + \hat{s}^y_j\hat{s}^y_{j+1}\right). \quad (2)$$

Here, the spin-operators $\hat{s}^\alpha_j = \hat{\sigma}^\alpha_j/2$ with Pauli matrices $\hat{\sigma}^\alpha$ are defined by $\hat{\sigma}^-_j = \hat{b}^\dagger_{j,\downarrow}\hat{b}_{j,\uparrow}$. The interaction strength $V_\perp \propto [1-3\cos^2(\theta)]$ is controlled by the angle θ between the field and the orientation of the 1D chain [Fig. 1(a)].

We assume that particles are prepared in their ground state $|\downarrow\rangle$ and uniformly distributed along the lattice such that each lattice site is occupied with probability $0 < f \leqslant 1$. Subsequently, a $\pi/2$ pulse prepares the dipoles in an x-polarized product state [see Fig. 1(b)] with density matrix $\hat{\rho}(t=0) = \bigotimes_j[(1-f)|0\rangle\langle 0|_j + f|{\rightarrow}\rangle\langle{\rightarrow}|_j]$, where $|0\rangle$ denotes an empty lattice site and $|{\rightarrow}\rangle = (|\uparrow\rangle + |\downarrow\rangle)/\sqrt{2}$.

The system's dynamics is described by the Lindblad master equation

$$\partial_t\hat{\rho} = \mathcal{L}\hat{\rho} = -i[\hat{H},\hat{\rho}] + \sum_j \mathcal{D}[\hat{L}_j]\hat{\rho}, \quad (3)$$

with $\mathcal{D}[\hat{L}]\hat{\rho} = 2\hat{L}\hat{\rho}\hat{L}^\dagger - \hat{L}^\dagger\hat{L}\hat{\rho} - \hat{\rho}\hat{L}^\dagger\hat{L}$. On-site two-body losses, e.g., due to chemical reactions are described by Lindblad operators of the form $\hat{L}_j = \sqrt{\Gamma/2}\hat{b}_{j,\downarrow}\hat{b}_{j,\uparrow}$, where the loss rate Γ increases with lattice depth [71,72]. We numerically simulate the dynamics of Eq. (3) by representing the vectorized density matrix as an infinite MPS directly in the thermodynamic limit, which we time-evolve with an infinite time evolving block-decimation algorithm [72,76–78]. We measure squeezing by the Wineland squeezing parameter, which quantifies the precision gain in a Ramsey spectroscopy experiment [25–27]

$$\xi^2 = \frac{N(\Delta S_\perp)^2_{\mathrm{min}}}{\langle\vec{S}\rangle^2}. \quad (4)$$

Here, $\vec{S} = \{\hat{S}^x, \hat{S}^y, \hat{S}^z\}$ with $\hat{S}^{\alpha=x,y,z} = \sum_j \hat{s}^\alpha_j$ is the Bloch vector, $4\langle\vec{S}\rangle^2/N^2 = 4\langle\hat{S}^x\rangle^2/N^2$ is the square of the contrast (since $\langle\hat{S}^y\rangle = \langle\hat{S}^z\rangle = 0$), and $(\Delta S_\perp)^2_{\mathrm{min}}$ is the minimal spin variance perpendicular to the Bloch vector [see illustration in Fig. 1(b)]. We use a method to compute squeezing from infinite MPSs directly in the thermodynamic limit, details of which are given in the Supplemental Material [72]. We confirm numerical convergence by generating all plots for successively increasing bond dimension up to a maximum of $\chi = 2048$ until convergence is reached [72].

In all figures, we use parameter values for fermionic KRb molecules in a magnetic field of ∼500 G at which the hyperfine splitting is $\gtrsim$100 kHz, which allows to energetically isolate a single hyperfine and rotational state pair [72]. In most of our analysis, we consider an angle $\theta \approx 59^\circ$ close to the magic angle. This reduces in-chain dipolar interactions by $[1-3\cos^2(\theta)]$ and makes it possible to tune the tunneling from much smaller to much larger than the dipolar interactions $J \gg V_\perp/J \ll V_\perp$. In the intermediate regime $J \sim V_\perp$, coupling between spin and motional degrees of freedom can introduce additional spin-motional entanglement, which would go beyond the scope of this paper.

Optimal parameter regimes. We start by discussing the numerical findings for $J_\uparrow = J_\downarrow = J$, and give an analytical

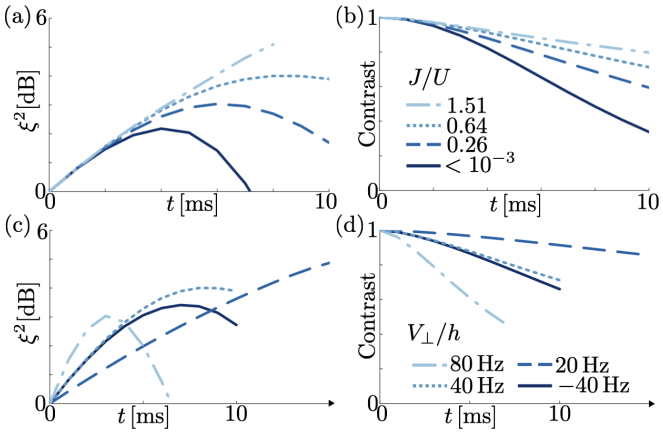

FIG. 2. Full system dynamics. Time evolution of (a) squeezing ξ^2 and (b) contrast for various lattice depths [from light to dark, $(V_{\mathrm{latt},x}, V_{\mathrm{latt},\perp})/E_R = (3,3), (3,40), (5,40), (40,40)$]. Parameters: $V_\perp/h = 40$ Hz, $f = 0.8$, $\Gamma = U_{\mathrm{contact}}/\hbar$. (c), (d) Same as (a) and (b) for varying dipolar interaction strength $V_\perp$, while keeping the on-site interaction, U, and loss rate, Γ, fixed, and $(V_{\mathrm{latt},x}, V_{\mathrm{latt},\perp})/E_R = (3,40)$. See the Supplemental Material for lattice and MPS parameters [72].

understanding in the following section. The maximal squeezing achieved within the first 10 ms is shown in Fig. 1(c) as a function of initial filling fraction and lattice depth. For all filling fractions, decreasing the lattice depth increases the squeezing. This is the main result of our paper and will be discussed below by considering time traces for parameters along the indicated arrows. We can see that while for deep lattices with frozen molecules ($J/U < 10^{-3}$), even for unit filling $f = 1$, squeezing is limited to around 3 dB, which constitutes a global maximum [see Fig. 3(a) below], shallow lattices can match and even out-perform these results for $f \gtrsim 0.4$. As will be discussed below in Fig. 4(b), for such small filling fractions squeezing is limited by the evolution time and does not constitute a global maximum, as indicated by the grey striped area. This implies that if times longer than 10 ms were considered, the results would shift even more in favor of shallow lattices at low filling since the apparent saturation with lattice depth for small f is limited only by the

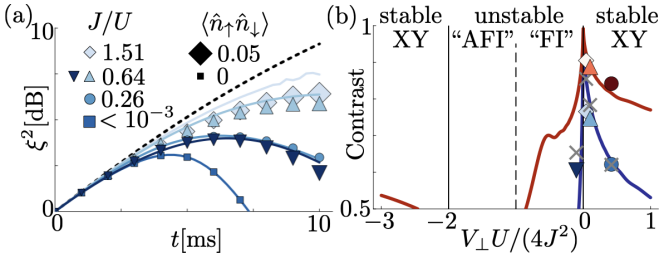

FIG. 3. Analytic models. (a) Spin squeezing dynamics for the FH model (symbols, size encodes doublon population), real-space spin-model (continuous lines), and the OAT limit (dotted line). (b) Contrast at 10 ms for spin-wave analysis (continuous lines; blue: $f = 1$; red: $f = 0.6$), spin model (gray x's; $f = 1$), and FH model (colored symbols; $f = 1$ without losses; $f = 0.6$ with losses). Vertical lines and text indicate stability of spin waves (see text).

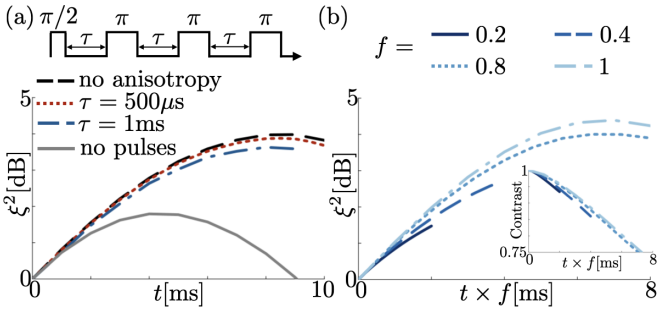

FIG. 4. Spin squeezing ξ^2 in the presence of imperfections. (a) X pulses with different pulse spacing τ protect against dephasing due to spin-dependent tunneling. We consider $J_\uparrow/h = 153$ Hz, $J_\downarrow/h = 131$ Hz compared to the no anisotropy reference with $J_\downarrow/h = J_\uparrow/h = 142$ Hz. Other parameters $f = 0.8$, $U_{\mathrm{contact}}/h = 529$ Hz, $U_{\mathrm{dd}/h} = -273$ Hz, $\Gamma = U_{\mathrm{contact}}/\hbar$, and $V_\perp/h = 40$ Hz. (b) Dynamics for different filling fractions f. Inset shows the contrast decay. Parameters: $J/h = 153$ Hz, $U/h = 239$ Hz, $\Gamma = 2\pi \times 512\mathrm{s}^{-1}$, and $V_\perp/h = 40$ Hz.

short-time growth, which we will show to be independent of lattice depth [Figs. 2(a) and 3(a)].

Figures 2(a) and 2(b) show the dynamics for different lattice depths at fixed filling $f = 0.8$. Changing the lattice depth modifies both tunneling rate and on-site interaction, such that a shallower lattice leads to a larger value of J/U. At short times, squeezing is generated at a rate independent of the lattice depth. For deep lattices, squeezing peaks at $\xi^2 \approx 2$ dB. In contrast, for shallower lattices when molecules are itinerant, the growth persists longer, leading to larger maximal squeezing at later times. This is mirrored in the contrast decay in panel (b). While for deep lattices the contrast decays quickly, it remains much larger for shallower lattices. One might expect that the larger on-site loss rate and faster contrast decay, and thus reduced Pauli blockade in deep lattices result in increased molecule loss. However, due to a combination of Zeno blockade and energetically suppressed doublon formation, the molecule loss is actually slowest in the deepest lattice. As a consequence, losses remain below 15% at all lattice depths [72].

Figures 2(c) and 2(d) show the squeezing dynamics for a range of dipolar interaction strengths $V_\perp$. First, focusing on the results for $V_\perp/h = 40$ Hz and $V_\perp/h = -40$ Hz, it is clear that positive values of $V_\perp$ are preferable; The growth of squeezing persists and the coherence is maintained longer. In order to observe the dependence on $|V_\perp|$, consider the curves for $V_\perp/h = (20, 40, 80)$ Hz. We find that increasing the interaction strength leads to a speed up of the dynamics, however at the cost of reducing the maximal squeezing. Maximum squeezing is thus achieved for shallow lattices and repulsive interactions. The optimal value of $|V_\perp|$ is then determined by any dephasing mechanisms, which set a time scale limiting how slow the dynamics can be made.

Analytical explanation. In order to gain insight into the underlying physics driving the results presented above, we now consider the lossless model with $\Gamma = 0$ in two complimentary limits. In the limit $J \gg U$, the dominant term in the Hamiltonian is the single-body term, which is diagonalized by Bloch waves, while scattering of Bloch waves can be

ignored to lowest order. In this case, for a finite number of lattice sites L, the dipole exchange interactions are projected into the Bloch wave basis, giving rise to all-to-all interactions described by a one-axis twisting Hamiltonian $(V_\perp/L)(\hat{S}^z)^2$ [72,79]. This Hamiltonian can be solved analytically and gives rise to squeezing limited only by finite Bloch sphere curvature effects, and unbounded squeezing in the limit $N \to \infty$ [27].

In the complementary limit $J \ll U$, $f = 1$, a combination of Pauli and interaction blockade mechanisms at small tunneling rates freezes dipole motion. In this regime, we can define an effective spin model by treating dipoles as localized spins [see Fig. 1(c)] [80]. The spins' interactions are governed by Eq. (2) and additional superexchange interactions from virtual hopping processes. The resulting Hamiltonian is an XXZ model given by:

$$\hat{H}_{\mathrm{sm}} = V_{\mathrm{sym,eff}} \sum_j \vec{s}_j \cdot \vec{s}_{j+1} + V_{z,\mathrm{eff}} \sum_j \hat{s}^z_j \hat{s}^z_{j+1} \tag{5}$$

with $V_{\mathrm{sym,eff}} = (4J^2/U) + V_\perp$ and $V_{z,\mathrm{eff}} = -V_\perp$ [72]. The term proportional to $V_{z,\mathrm{eff}}$ generates spin squeezing identical to one-axis twisting at short times, but leads to dephasing on longer time scales. In contrast, the term proportional $V_{\mathrm{sym,eff}}$ in Eq. (5) is SU(2) symmetric and thus cannot generate squeezing by itself, but favors spin alignment, thus suppressing dephasing introduced by $V_{z,\mathrm{eff}}$.

The resulting squeezing as predicted by both spin models is compared to the FH model in Fig. 3(a). While at short times all descriptions predict identical squeezing, at later times the real-space spin model predicts reduced squeezing compared to the fully collective momentum space spin model, and matches the full model for $J/U \lesssim 0.3$. For shallower lattices squeezing is reduced compared to the spin models. This breakdown of the spin model coincides with a rise in doubly occupied sites [Fig. 3(a) size of blue symbols], which moves the system out of the spin model manifold, and direct motion of molecules is nonnegligible. We note that for all parameters analyzed here, the real-space spin model gives more accurate results than the momentum-space spin model, which is only accurate at short times.

In the regime of validity of the spin model, squeezing is limited by loss of contrast. To shed light on this effect, we solve the dynamics of spin-waves at short times. We map each spin to a hard-core boson according to the mapping: $|{\rightarrow}\rangle_n = |0\rangle_n$ and $|{\leftarrow}\rangle_n = |1\rangle_n$ for $|0\rangle_n$ and $|1\rangle_n$ states representing zero and one bosons on site n, respectively. This allows for the reduction of the spin model to a quadratic Hamiltonian that can be solved by a Bogoliubov transformation [72]. The resulting dynamics describes pair creation of spin waves with momenta k and $-k$, which maps for $|k| \neq 0$ to contrast decay proportional to the number of spin-wave excitations.

The predicted contrast after 10 ms is shown in Fig. 3(b) (red line). We find that the contrast remains large for $V_\perp U/(4J^2) > 0$, and quickly approaches one as $V_\perp U/(4J^2) \to 0$. While the spin-wave analysis accurately predicts the contrast for $V_\perp U/(4J^2) > 0$, the contrast is slightly underestimated for $V_\perp U/(4J^2) < 0$. The quantitative discrepancy is caused by the terms neglected under the spin-wave approximation. To lowest order, we can account for subunit filling by re-scaling all interaction constants with the filling fraction $V_{\mathrm{sym,eff}} \to f V_{\mathrm{sym,eff}}$ and $V_{z,\mathrm{eff}} \to f V_{z,\mathrm{eff}}$ due to a reduction of the average (mean-field) interactions. The blue line and symbols in Fig. 3(b) show that this rescaling accurately captures the contrast, even when losses are included in the full model.

The asymmetry around $V_\perp U/(4J^2) = 0$ can be understood from a stability analysis of the spin waves [72]. For $V_\perp U/(4J^2) > 0$ and $V_\perp U/(4J^2) < -2$, all modes are stable, such that pair creation remains small and contrast remains large. In contrast, for $-2 < V_\perp U/(4J^2) < 0$, some modes become unstable and contrast decays quickly. In line with prior work [45,48], we can draw a connection between contrast protection and the relevant phase diagram close to negative zero temperature, i.e., the ground state phase diagram of the negative Hamiltonian. In the stable regime, the ground state has short-range XY-order, forcing spins to stay aligned. In contrast, for $-1 < V_\perp U/(4J^2) < 0$, the ground state has short-range ferromagnetic Ising order, and modes close to $k = 0$ are unstable, and for $-2 < V_\perp U/(4J^2) < -1$ the ground state has short-range antiferromagnetic Ising order, and modes with quasimomentum $2\pi k/N \approx \pi$ are unstable.

Experimental considerations. Finally, we consider the impact of experimental imperfections on the generation of squeezing in Fig. 4. Panel (a) shows the effect of spin-dependent tunneling rates, and panel (b) shows different filling fractions. Spin dephasing naturally arises due to the distinct polarizabilities of the spin states and the resulting state-dependent trapping potentials and tunneling rates $J_\uparrow \neq J_\downarrow$. Typical values for KRb at a lattice depth of $3E_R$ for the $|\uparrow\rangle$ state are $J_\uparrow/h = 153$ Hz and $J_\downarrow/h = 131$ Hz [72]. In Fig. 4(a) we find that this leads to a reduction of spin squeezing from $\sim$4 dB to $\sim$2 dB. The tunneling anisotropy can in principle be removed by a dynamical decoupling sequence, which effectively averages the tunneling rates of both states [23,24,59]. Here, we consider a sequence of (infinitely fast) π pulses along x, $\exp(\mathrm{i}\pi\hat{S}^x)$, spaced by a time τ, and find that pulses with a pulse spacing of $\tau = 500\,\mu$s are sufficient to almost fully recover the peak squeezing.

Panel (b) shows the squeezing dynamics at different filling fractions, corresponding to a horizontal cut through the diagram in Fig. 1(c), versus time scaled by the initial filling fraction. In experiments, the filling fraction is limited by the temperature of the gas before loading it into a lattice. We can compute the maximal achievable filling fraction by matching the entropy of free space gases to the entropy in the respective optical lattice. While so far experiments in optical lattices have achieved filling fractions up to $f = 0.25$ [81], for $T/T_F = 0.3$ as reported in Ref. [11], filling fractions up to $f = 0.9$ should be reachable in near term experiments [82].

We observe a collapse of all curves when plotted as a function of the rescaled time $t \times f$. The slowdown of the dynamics is due to the reduction of the average interactions $\propto f$. At later times, systems with lower filling fractions have reduced squeezing compared to the $f = 1$ case, indicating that small filling fractions reduce the maximal attainable squeezing. Since the contrast is barely affected, the reduction in squeezing is due to an increase in the variance in Eq. (4), which may be, e.g., due to enhanced motion at lower filling or disorder in the initial state. Nevertheless, the most important

reduction of the maximally reported spin squeezing for smaller filling fractions in Fig. 1(c) is imposed by the runtime of the dynamics, which here we set to 10 ms, but will ultimately be limited by additional sources of spin dephasing in an experiment. Previous experiments in pancakes had coherence times limited by collisions [59] which are already included in our analysis. In a lattice, interaction-limited spin coherence times can be larger than 400 ms [22], leading to negligible coherence loss on the 10 ms time scales considered here [72], thus supporting the possibility to generate several dB squeezing in current experiments.

We nevertheless emphasize that the contrast stabilization due to superexchange is potentially reduced at low filling fractions. The reason behind this is that for very low filling fractions, the spin dynamics become increasingly dominated by pairs of closeby dipoles isolated from the rest of the system. For such pairs, superexchange and spin-exchange interactions commute $[\vec{s}_i \cdot \vec{s}_j, \hat{s}_i^+ \hat{s}_j^- + \text{H.c.}] = 0$, and therefore, superexchange cannot modify the contrast decay induced by dipolar spin-exchange interactions. For example, filling fractions larger than 15% are required to stabilize the contrast of frozen dipoles in 2D [83].

Conclusion. Our results demonstrate that spin squeezing is maximal in shallow lattices. While our study is focused on 1D due to the availability of exact numerical methods, we note that the derivation of the spin-model is independent of the dimensionality, suggesting that our results remain true for higher dimensions as long as the interactions are isotropic. This is relevant for future experiments, where two-dimensional systems may be more natural to implement. Furthermore, previous studies have shown that spin squeezing in higher dimensions is much larger and can scale with system size [45,48], but is also limited by low filling fractions [83]. Larger $\vec{E}$ fields and Floquet engineering provide additional tuning knobs, which can turn the XY into an XXZ model [74,84], and thus further control $V_{z,\text{eff}}$. Additional density-spin interaction terms [73] for large $\vec{E}$ fields may constitute an additional source of dephasing, which can however be removed by the pulse sequence discussed in Fig. 4(a). While we focused on fermionic dipoles, it is an interesting prospect to consider if our results can be further extended to bosons [85], and how they ultimately translate when pushing to even shallower lattices when corrections to the Fermi-Hubbard model become important [86,87].

Acknowledgments. We acknowledge careful review of this manuscript and useful comments from Jun-Ru Li and Jacob Higgins. We thank Johannes Schachenmayer for valuable contributions to the MPS code, which makes use of the intelligent tensor library (ITensor) [88], written in the julia programming language [89]. The work is supported by the AFOSR MURI, the ARO single investigator Award No. W911NF-19-1-0210, Grant No. NSF JILA-PFC PHY-2317149, QLCI-OMA-2016244, by the U.S. Department of Energy, Office of Science, National Quantum Information Science Research Centers Quantum Systems Accelerator, and NIST.

[1] M. A. Baranov, M. Dalmonte, G. Pupillo, and P. Zoller, Condensed matter theory of dipolar quantum gases, Chem. Rev. **112**, 5012 (2012).

[2] S. A. Moses, J. P. Covey, M. T. Miecnikowski, D. S. Jin, and J. Ye, New frontiers for quantum gases of polar molecules, Nat. Phys. **13**, 13 (2017).

[3] J. L. Bohn, A. M. Rey, and J. Ye, Cold molecules: Progress in quantum engineering of chemistry and quantum matter, Science **357**, 1002 (2017).

[4] L. Chomaz, I. Ferrier-Barbut, F. Ferlaino, B. Laburthe-Tolra, B. L. Lev, and T. Pfau, Dipolar physics: A review of experiments with magnetic quantum gases, Rep. Prog. Phys. **86**, 026401 (2023).

[5] A. Browaeys and T. Lahaye, Many-body physics with individually controlled Rydberg atoms, Nat. Phys. **16**, 132 (2020).

[6] M. Morgado and S. Whitlock, Quantum simulation and computing with Rydberg-interacting qubits, AVS Quantum Sci. **3**, 023501 (2021).

[7] K.-K. Ni, S. Ospelkaus, M. H. G. de Miranda, A. Pe'er, B. Neyenhuis, J. J. Zirbel, S. Kotochigova, P. S. Julienne, D. S. Jin, and J. Ye, A high phase-space-density gas of polar molecules, Science **322**, 231 (2008).

[8] M. Lu, N. Q. Burdick, S. H. Youn, and B. L. Lev, Strongly dipolar Bose-einstein condensate of dysprosium, Phys. Rev. Lett. **107**, 190401 (2011).

[9] K. Aikawa, A. Frisch, M. Mark, S. Baier, A. Rietzler, R. Grimm, and F. Ferlaino, Bose-einstein condensation of erbium, Phys. Rev. Lett. **108**, 210401 (2012).

[10] T. Takekoshi, L. Reichsöllner, A. Schindewolf, J. M. Hutson, C. R. Le Sueur, O. Dulieu, F. Ferlaino, R. Grimm, and H.-C. Nägerl, Ultracold dense samples of dipolar RbCs molecules in the rovibrational and hyperfine ground state, Phys. Rev. Lett. **113**, 205301 (2014).

[11] L. De Marco, G. Valtolina, K. Matsuda, W. G. Tobias, J. P. Covey, and J. Ye, A degenerate Fermi gas of polar molecules, Science **363**, 853 (2019).

[12] G. A. Phelps, A. Hébert, A. Krahn, S. Dickerson, F. Öztürk, S. Ebadi, L. Su, and M. Greiner, Sub-second production of a quantum degenerate gas, arXiv:2007.10807.

[13] H. Son, J. J. Park, W. Ketterle, and A. O. Jamison, Collisional cooling of ultracold molecules, Nature (London) **580**, 197 (2020).

[14] K. Matsuda, L. De Marco, J.-R. Li, W. G. Tobias, G. Valtolina, G. Quéméner, and J. Ye, Resonant collisional shielding of reactive molecules using electric fields, Science **370**, 1324 (2020).

[15] K. K. Voges, P. Gersema, M. M. zum Alten Borgloh, T. A. Schulze, T. Hartmann, A. Zenesini, and S. Ospelkaus, Ultracold gas of Bosonic ^{23}Na^{39}K ground-state molecules, Phys. Rev. Lett. **125**, 083401 (2020).

[16] E. Guardado-Sanchez, B. M. Spar, P. Schauss, R. Belyansky, J. T. Young, P. Bienias, A. V. Gorshkov, T. Iadecola, and W. S. Bakr, Quench dynamics of a Fermi gas with strong nonlocal interactions, Phys. Rev. X **11**, 021036 (2021).

[17] A. Schindewolf, R. Bause, X.-Y. Chen, M. Duda, T. Karman, I. Bloch, and X.-Y. Luo, Evaporation of microwave-shielded polar

molecules to quantum degeneracy, Nature (London) **607**, 677 (2022).
[18] I. Stevenson, A. Z. Lam, N. Bigagli, C. Warner, W. Yuan, S. Zhang, and S. Will, Ultracold gas of dipolar NaCs ground state molecules, Phys. Rev. Lett. **130**, 113002 (2023).
[19] L. Anderegg, L. W. Cheuk, Y. Bao, S. Burchesky, W. Ketterle, K.-K. Ni, and J. M. Doyle, An optical tweezer array of ultracold molecules, Science **365**, 1156 (2019).
[20] J. T. Zhang, Y. Yu, W. B. Cairncross, K. Wang, L. R. B. Picard, J. D. Hood, Y.-W. Lin, J. M. Hutson, and K.-K. Ni, Forming a single molecule by magnetoassociation in an optical tweezer, Phys. Rev. Lett. **124**, 253401 (2020).
[21] S. Burchesky, L. Anderegg, Y. Bao, S. S. Yu, E. Chae, W. Ketterle, K.-K. Ni, and J. M. Doyle, Rotational coherence times of polar molecules in optical tweezers, Phys. Rev. Lett. **127**, 123202 (2021).
[22] L. Christakis, J. S. Rosenberg, R. Raj, S. Chi, A. Morningstar, D. A. Huse, Z. Z. Yan, and W. S. Bakr, Probing site-resolved correlations in a spin system of ultracold molecules, Nature **614**, 64 (2023).
[23] C. M. Holland, Y. Lu, and L. W. Cheuk, On-demand entanglement of molecules in a reconfigurable optical tweezer array, Science **382**, 1143 (2023).
[24] Y. Bao, S. S. Yu, L. Anderegg, E. Chae, W. Ketterle, K.-K. Ni, and J. M. Doyle, Dipolar spin-exchange and entanglement between molecules in an optical tweezer array, Science **382**, 1138 (2023).
[25] D. J. Wineland, J. J. Bollinger, W. M. Itano, F. L. Moore, and D. J. Heinzen, Spin squeezing and reduced quantum noise in spectroscopy, Phys. Rev. A **46**, R6797 (1992).
[26] D. J. Wineland, J. J. Bollinger, W. M. Itano, and D. J. Heinzen, Squeezed atomic states and projection noise in spectroscopy, Phys. Rev. A **50**, 67 (1994).
[27] J. Ma, X. Wang, C. P. Sun, and F. Nori, Quantum spin squeezing, Phys. Rep. **509**, 89 (2011).
[28] A. Sørensen, L.-M. Duan, J. I. Cirac, and P. Zoller, Many-particle entanglement with Bose–Einstein condensates, Nature (London) **409**, 63 (2001).
[29] L. Pezzè, A. Smerzi, M. K. Oberthaler, R. Schmied, and P. Treutlein, Quantum metrology with nonclassical states of atomic ensembles, Rev. Mod. Phys. **90**, 035005 (2018).
[30] J. Appel, P. J. Windpassinger, D. Oblak, U. B. Hoff, N. Kjærgaard, and E. S. Polzik, Mesoscopic atomic entanglement for precision measurements beyond the standard quantum limit, Proc. Natl. Acad. Sci. USA **106**, 10960 (2009).
[31] R. J. Sewell, M. Koschorreck, M. Napolitano, B. Dubost, N. Behbood, and M. W. Mitchell, Magnetic sensitivity beyond the projection noise limit by spin squeezing, Phys. Rev. Lett. **109**, 253605 (2012).
[32] C. D. Hamley, C. S. Gerving, T. M. Hoang, E. M. Bookjans, and M. S. Chapman, Spin-nematic squeezed vacuum in a quantum gas, Nat. Phys. **8**, 305 (2012).
[33] W. Muessel, H. Strobel, D. Linnemann, D. B. Hume, and M. K. Oberthaler, Scalable spin squeezing for quantum-enhanced magnetometry with Bose-einstein condensates, Phys. Rev. Lett. **113**, 103004 (2014).
[34] J. G. Bohnet, K. C. Cox, M. A. Norcia, J. M. Weiner, Z. Chen, and J. K. Thompson, Reduced spin measurement back-action for a phase sensitivity ten times beyond the standard quantum limit, Nat. Photon. **8**, 731 (2014).
[35] R. Schmied, J.-D. Bancal, B. Allard, M. Fadel, V. Scarani, P. Treutlein, and N. Sangouard, Bell correlations in a Bose-Einstein condensate, Science **352**, 441 (2016).
[36] I. Kruse, K. Lange, J. Peise, B. Lücke, L. Pezzè, J. Arlt, W. Ertmer, C. Lisdat, L. Santos, A. Smerzi, and C. Klempt, Improvement of an atomic clock using squeezed vacuum, Phys. Rev. Lett. **117**, 143004 (2016).
[37] K. C. Cox, G. P. Greve, J. M. Weiner, and J. K. Thompson, Deterministic squeezed states with collective measurements and feedback, Phys. Rev. Lett. **116**, 093602 (2016).
[38] O. Hosten, N. J. Engelsen, R. Krishnakumar, and M. A. Kasevich, Measurement noise 100 times lower than the quantum-projection limit using entangled atoms, Nature (London) **529**, 505 (2016).
[39] J. G. Bohnet, B. C. Sawyer, J. W. Britton, M. L. Wall, A. M. Rey, M. Foss-Feig, and J. J. Bollinger, Quantum spin dynamics and entanglement generation with hundreds of trapped ions, Science **352**, 1297 (2016).
[40] S. Baier, M. J. Mark, D. Petter, K. Aikawa, L. Chomaz, Z. Cai, M. Baranov, P. Zoller, and F. Ferlaino, Extended Bose-Hubbard models with ultracold magnetic atoms, Science **352**, 201 (2016).
[41] T. Chalopin, C. Bouazza, A. Evrard, V. Makhalov, D. Dreon, J. Dalibard, L. A. Sidorenkov, and S. Nascimbene, Quantum-enhanced sensing using non-classical spin states of a highly magnetic atom, Nat. Commun. **9**, 4955 (2018).
[42] B. Braverman, A. Kawasaki, E. Pedrozo-Peñafiel, S. Colombo, C. Shu, Z. Li, E. Mendez, M. Yamoah, L. Salvi, D. Akamatsu, Y. Xiao, and V. Vuletić, Near-unitary spin squeezing in ^{171}Yb, Phys. Rev. Lett. **122**, 223203 (2019).
[43] H. Bao, J. Duan, S. Jin, X. Lu, P. Li, W. Qu, M. Wang, I. Novikova, E. E. Mikhailov, K.-F. Zhao, K. Mølmer, H. Shen, and Y. Xiao, Spin squeezing of 1011 atoms by prediction and retrodiction measurements, Nature (London) **581**, 159 (2020).
[44] E. Pedrozo-Peñafiel, S. Colombo, C. Shu, A. F. Adiyatullin, Z. Li, E. Mendez, B. Braverman, A. Kawasaki, D. Akamatsu, Y. Xiao, and V. Vuletić, Entanglement on an optical atomic-clock transition, Nature (London) **588**, 414 (2020).
[45] M. A. Perlin, C. Qu, and A. M. Rey, Spin squeezing with short-range spin-exchange interactions, Phys. Rev. Lett. **125**, 223401 (2020), see Supplemental for 1D.
[46] M. Mamaev, I. Kimchi, R. M. Nandkishore, and A. M. Rey, Tunable-spin-model generation with spin-orbit-coupled fermions in optical lattices, Phys. Rev. Res. **3**, 013178 (2021).
[47] T. Hernández Yanes, M. Płodzień, M. Mackoit Sinkevičienė, G. Žlabys, G. Juzeliūnas, and E. Witkowska, One- and two-axis squeezing via laser coupling in an atomic fermi-hubbard model, Phys. Rev. Lett. **129**, 090403 (2022).
[48] M. Block, B. Ye, B. Roberts, S. Chern, W. Wu, Z. Wang, L. Pollet, E. J. Davis, B. I. Halperin, and N. Y. Yao, A universal theory of spin squeezing, arXiv:2301.09636.
[49] B. Yan, S. A. Moses, B. Gadway, J. P. Covey, K. R. A. Hazzard, A. M. Rey, D. S. Jin, and J. Ye, Observation of dipolar spin-exchange interactions with lattice-confined polar molecules, Nature (London) **501**, 521 (2013).
[50] F. Seeßelberg, X.-Y. Luo, M. Li, R. Bause, S. Kotochigova, I. Bloch, and C. Gohle, Extending rotational coherence of interacting polar molecules in a spin-decoupled magic trap, Phys. Rev. Lett. **121**, 253401 (2018).

[51] S. Lepoutre, J. Schachenmayer, L. Gabardos, B. Zhu, B. Naylor, E. Maréchal, O. Gorceix, A. M. Rey, L. Vernac, and B. Laburthe-Tolra, Out-of-equilibrium quantum magnetism and thermalization in a spin-3 many-body dipolar lattice system, Nat. Commun. **10**, 1714 (2019).

[52] A. Patscheider, B. Zhu, L. Chomaz, D. Petter, S. Baier, A.-M. Rey, F. Ferlaino, and M. J. Mark, Controlling dipolar exchange interactions in a dense three-dimensional array of large-spin fermions, Phys. Rev. Res. **2**, 023050 (2020).

[53] J. Lin, J. He, M. Jin, G. Chen, and D. Wang, Seconds-scale coherence on nuclear spin transitions of ultracold polar molecules in 3D optical lattices, Phys. Rev. Lett. **128**, 223201 (2022).

[54] Y. A. Alaoui, B. Zhu, S. R. Muleady, W. Dubosclard, T. Roscilde, A. M. Rey, B. Laburthe-Tolra, and L. Vernac, Measuring correlations from the collective spin fluctuations of a large ensemble of lattice-trapped dipolar spin-3 atoms, Phys. Rev. Lett. **129**, 023401 (2022).

[55] W. J. Eckner, N. D. Oppong, A. Cao, A. W. Young, W. R. Milner, J. M. Robinson, J. Ye, and A. M. Kaufman, Realizing spin squeezing with Rydberg interactions in an optical clock, Nature **621**, 734 (2023).

[56] J. A. Hines, S. V. Rajagopal, G. L. Moreau, M. D. Wahrman, N. A. Lewis, O. Marković, and M. Schleier-Smith, Spin squeezing by Rydberg dressing in an array of atomic ensembles, Phys. Rev. Lett. **131**, 063401 (2023).

[57] J. Franke, S. R. Muleady, R. Kaubruegger, F. Kranzl, R. Blatt, A. M. Rey, M. K. Joshi, and C. F. Roos, Quantum-enhanced sensing on an optical transitions through finite-range interactions, Nature **621**, 740 (2023).

[58] G. Bornet, G. Emperauger, C. Chen, B. Ye, M. Block, M. Bintz, J. A. Boyd, D. Barredo, T. Comparin, F. Mezzacapo, T. Roscilde, T. Lahaye, N. Y. Yao, and A. Browaeys, Scalable spin squeezing in a dipolar Rydberg atom array, Nature **621**, 728 (2023).

[59] J.-R. Li, K. Matsuda, C. Miller, A. N. Carroll, W. G. Tobias, J. S. Higgins, and J. Ye, Tunable itinerant spin dynamics with polar molecules, Nature (London) **614**, 70 (2023).

[60] T. Bilitewski, L. De Marco, J.-R. Li, K. Matsuda, W. G. Tobias, G. Valtolina, J. Ye, and A. M. Rey, Dynamical generation of spin squeezing in ultracold dipolar molecules, Phys. Rev. Lett. **126**, 113401 (2021).

[61] Z. Idziaszek and P. S. Julienne, Universal rate constants for reactive collisions of ultracold molecules, Phys. Rev. Lett. **104**, 113202 (2010).

[62] G. Quéméner, J. L. Bohn, A. Petrov, and S. Kotochigova, Universalities in ultracold reactions of alkali-metal polar molecules, Phys. Rev. A **84**, 062703 (2011).

[63] J. F. E. Croft, J. L. Bohn, and G. Quéméner, Unified model of ultracold molecular collisions, Phys. Rev. A **102**, 033306 (2020).

[64] P. D. Gregory, J. A. Blackmore, D. Frye Matthew, L. M. Fernley, S. L. Bromley, J. M. Hutson, and S. L. Cornish, Molecule-molecule and atom-molecule collisions with ultracold RbCs molecules, New J. Phys. **23**, 125004 (2021).

[65] S. L. Cornish and J. M. Hutson, Toward a coherent ultracold chemistry, Science **375**, 975 (2022).

[66] Y. Liu and K.-K. Ni, Bimolecular chemistry in the ultracold regime, Annu. Rev. Phys. Chem. **73**, 73 (2022).

[67] R. Bause, A. Christianen, A. Schindewolf, I. Bloch, and X.-Y. Luo, Ultracold sticky collisions: Theoretical and experimental status, J. Phys. Chem. A **127**, 729 (2023).

[68] A. de Paz, P. Pedri, A. Sharma, M. Efremov, B. Naylor, O. Gorceix, E. Maréchal, L. Vernac, and B. Laburthe-Tolra, Probing spin dynamics from the Mott insulating to the superfluid regime in a dipolar lattice gas, Phys. Rev. A **93**, 021603(R) (2016).

[69] P. Fersterer, A. Safavi-Naini, B. Zhu, L. Gabardos, S. Lepoutre, L. Vernac, B. Laburthe-Tolra, P. B. Blakie, and A. M. Rey, Dynamics of an itinerant spin-3 atomic dipolar gas in an optical lattice, Phys. Rev. A **100**, 033609 (2019).

[70] K. Sponselee, L. Freystatzky, B. Abeln, M. Diem, B. Hundt, A. Kochanke, T. Ponath, B. Santra, L. Mathey, K. Sengstock, and C. Becker, Dynamics of ultracold quantum gases in the dissipative Fermi–Hubbard model, Quantum Sci. Technol. **4**, 014002 (2018).

[71] B. Zhu, B. Gadway, M. Foss-Feig, J. Schachenmayer, M. L. Wall, K. R. A. Hazzard, B. Yan, S. A. Moses, J. P. Covey, D. S. Jin, J. Ye, M. Holland, and A. M. Rey, Suppressing the loss of ultracold molecules via the continuous quantum zeno effect, Phys. Rev. Lett. **112**, 070404 (2014).

[72] See Supplemental Material at http://link.aps.org/supplemental/10.1103/PhysRevResearch.6.L012025 for details on the model and its derivation, numerical simulations, the spin model, and the effect of losses and dephasing, which includes Refs. [7,49,61,71,73,75–77,86,90–97].

[73] A. V. Gorshkov, S. R. Manmana, G. Chen, E. Demler, M. D. Lukin, and A. M. Rey, Quantum magnetism with polar alkali-metal dimers, Phys. Rev. A **84**, 033619 (2011).

[74] A. V. Gorshkov, S. R. Manmana, G. Chen, J. Ye, E. Demler, M. D. Lukin, and A. M. Rey, Tunable superfluidity and quantum magnetism with ultracold polar molecules, Phys. Rev. Lett. **107**, 115301 (2011).

[75] B. Neyenhuis, B. Yan, S. A. Moses, J. P. Covey, A. Chotia, A. Petrov, S. Kotochigova, J. Ye, and D. S. Jin, Anisotropic polarizability of ultracold polar ^{40}K ^{87}Rb molecules, Phys. Rev. Lett. **109**, 230403 (2012).

[76] R. Orús and G. Vidal, Infinite time-evolving block decimation algorithm beyond unitary evolution, Phys. Rev. B **78**, 155117 (2008).

[77] U. Schollwöck, The density-matrix renormalization group in the age of matrix product states, Ann. Phys. **326**, 96 (2011).

[78] H. Weimer, A. Kshetrimayum, and R. Orús, Simulation methods for open quantum many-body systems, Rev. Mod. Phys. **93**, 015008 (2021).

[79] P. He, M. A. Perlin, S. R. Muleady, R. J. Lewis-Swan, R. B. Hutson, J. Ye, and A. M. Rey, Engineering spin squeezing in a 3D optical lattice with interacting spin-orbit-coupled fermions, Phys. Rev. Res. **1**, 033075 (2019).

[80] A. A. Abrikosov, Electron scattering on magnetic impurities in metals and anomalous resistivity effects, Phys. Phys. Fiz. **2**, 5 (1965).

[81] S. A. Moses, J. P. Covey, M. T. Miecnikowski, B. Yan, B. Gadway, J. Ye, and D. S. Jin, Creation of a low-entropy quantum gas of polar molecules in an optical lattice, Science **350**, 659 (2015).

[82] A 3D harmonic oscillator at $T/T_F = 0.3$ has $S/(Nk_B) \approx 0.37$. A uniform filling fraction with $f = 0.9$ has $S/(Nk_B) = -\ln(f) - (1-f)\ln(1-f)/f = 0.36$.

[83] M. P. Kwasigroch and N. R. Cooper, Synchronization transition in dipole-coupled two-level systems with positional disorder, Phys. Rev. A **96**, 053610 (2017).

[84] P. Scholl, H. J. Williams, G. Bornet, F. Wallner, D. Barredo, L. Henriet, A. Signoles, C. Hainaut, T. Franz, S. Geier, A. Tebben, A. Salzinger, G. Zürn, T. Lahaye, M. Weidemüller, and A. Browaeys, Microwave engineering of programmable XXZ Hamiltonians in arrays of Rydberg atoms, PRX Quantum **3**, 020303 (2022).

[85] M. Dziurawiec, T. H. Yanes, M. Płodzień, M. Gajda, M. Lewenstein, and E. Witkowska, Accelerating many-body entanglement generation by dipolar interactions in the Bose-Hubbard model, Phys. Rev. A **107**, 013311 (2023).

[86] M. L. Wall, N. P. Mehta, R. Mukherjee, S. S. Alam, and K. R. A. Hazzard, Microscopic derivation of multichannel Hubbard models for ultracold nonreactive molecules in an optical lattice, Phys. Rev. A **95**, 043635 (2017).

[87] M. Hughes, A. U. J. Lode, D. Jaksch, and P. Molignini, Accuracy of quantum simulators with ultracold dipolar molecules: A quantitative comparison between continuum and lattice descriptions, Phys. Rev. A **107**, 033323 (2023).

[88] M. Fishman, S. R. White, and E. M. Stoudenmire, The ITensor software library for tensor network calculations, SciPost Phys. Codebases 4 (2022).

[89] J. Bezanson, A. Edelman, S. Karpinski, and V. B. Shah, Julia: A fresh approach to numerical computing, SIAM Rev. **59**, 65 (2017).

[90] I. Bloch, J. Dalibard, and W. Zwerger, Many-body physics with ultracold gases, Rev. Mod. Phys. **80**, 885 (2008).

[91] J. J. García-Ripoll, S. Dürr, N. Syassen, D. M. Bauer, M. Lettner, G. Rempe, and J. I. Cirac, Dissipation-induced hard-core boson gas in an optical lattice, New J. Phys. **11**, 013053 (2009).

[92] A. T. Sornborger and E. D. Stewart, Higher-order methods for simulations on quantum computers, Phys. Rev. A **60**, 1956 (1999).

[93] F. Reiter and A. S. Sørensen, Effective operator formalism for open quantum systems, Phys. Rev. A **85**, 032111 (2012).

[94] J. M. Hutson, Feshbach resonances in ultracold atomic and molecular collisions: threshold behaviour and suppression of poles in scattering lengths, New J. Phys. **9**, 152 (2007).

[95] M. H. G. de Miranda, A. Chotia, B. Neyenhuis, D. Wang, G. Quéméner, S. Ospelkaus, J. L. Bohn, J. Ye, and D. S. Jin, Controlling the quantum stereodynamics of ultracold bimolecular reactions, Nat. Phys. **7**, 502 (2011).

[96] G. Preisser, D. Wellnitz, T. Botzung, and J. Schachenmayer, Comparing bipartite entropy growth in open-system matrix-product simulation methods, Phys. Rev. A **108**, 012616 (2023).

[97] G. Wójtowicz, J. E. Elenewski, M. M. Rams, and M. Zwolak, Open-system tensor networks and Kramers' crossover for quantum transport, Phys. Rev. A **101**, 050301(R) (2020).